www.sciencemag.org/content/363/6431/1098/suppl/DC1

# Supplementary Materials for

## A molecular assembly phase transition and kinetic proofreading modulate Ras activation by SOS

William Y. C. Huang, Steven Alvarez*, Yasushi Kondo*, Young Kwang Lee, Jean K. Chung, Hiu Yue Monatrice Lam, Kabir H. Biswas, John Kuriyan, Jay T. Groves†

*These authors contributed equally to this work.
†Corresponding author. Email: jtgroves@lbl.gov

Published 8 March 2019, *Science* **363**, 1098 (2019)
DOI: 10.1126/science.aau5721

**This PDF file includes:**



**Other Supplementary Material for this manuscript includes the following:**
(available at www.sciencemag.org/content/363/6431/1098/suppl/DC1)

## Materials and Methods

Chemicals

1,2-dioleoyl-sn-glycero-3-phosphocholine (DOPC) and 1,2-dioleoyl-sn-glycero-3-[(N-(5-amino-1-carboxypentyl)iminodiacetic acid)succinyl] (nickel salt) ($Ni^{2+}$-NTA-DOGS) were purchased from Avanti Polar Lipids. Texas Red 1,2-dihexadecanoylsn-glycero-3-phosphoethanolamine (TR-DHPE) was purchased from Invitrogen. Alexa Fluor 647 maleimide dye and Alexa Fluor 561 maleimide dye were purchased from Life Technology. Bovine Serum Albumin (BSA), (±)-6-Hydroxy-2,5,7,8-tetramethylchromane-2-carboxylic acid (Trolox), Catalase, 2-Mercaptoethanol (BME), $NiCl_2$, $H_2SO_4$ and ATP were purchased from Sigma-Aldrich. Glucose Oxidase was purchased from Serva. Tris(2-carboxyethyl)phosphine (TCEP) was brought from Thermo Scientific. Glucose and $H_2O_2$ were from Fisher Scientific. $MgCl_2$ was from EMD Chemicals. Tris buffer saline (TBS) was purchased from Corning.

Protein purification

***LAT and Grb2*** Human LAT cytosolic domain (residues 30 to 233) and full-length Grb2 were purified as described previously (48) using an N-terminal 6-His tag. For Grb2, the N-terminal 6-His tag was removed with Tobacco Etch Virus protease.

***Ras*** H-RasC118S (residue 1-181) was purified as described previously (19) using an N-terminal 6-His tag. The N-terminal 6-His tag was removed with Tobacco Etch Virus protease.

***$SOS^{FL}$*** Expression and purification of full-length SOS protein ($SOS^{FL}$) from a bacterial expression system was unsuccessful as severe proteolysis would occur. In order to prevent proteolysis during the purification step, we used a split intein approach where we purified the N- and the C-terminal fragments of human SOS1 separately and to high purity. We then used the intein reaction to ligate the two fragments together (35) followed by another step of purification of the full-length protein.

The boundary between the N- and C-terminal fragments of SOS was placed in-between the CDC25 and PR domains (Fig. 1A), in a region that is predicted to be disordered. The amino-terminal SOS fragment ($SOS^{N}$; residues 2-1048) was cloned into a 2S-T vector containing an aminoterminal 6xHisSUMO tag (Addgene #29711). An amino-terminal consensus fast DnaE intein sequence (CfaN; (35)) followed by a monomeric Ocr fusion tag (49) was cloned following the carboxy-terminus of SOS-N. Mocr domain is highly acidic, and the addition of the domain helped the separation of $SOS^{FL}$ from unreacted $SOS^{N}$ during the final purification on the MonoQ column (see below). The carboxy-terminal SOS fragment ($SOS^{C}$; residues 1049-1333) was cloned into a vector containing a hexahistidine tag followed by a TEV protease cleavage site and a NpuC intein sequence (50). The NpuC plasmid was a kind gift of Dr. Shah. Two mutations are added to the $SOS^{C}$ sequence: T1049C introduced a catalytic cysteine residue for the intein reaction, and M1050F brought the preferable +2 residue for the efficient intein reaction (35).

Both fragments were overexpressed in Rosetta2(DE3) cells (Novagen). The transformed cells were grown at 37˚C in Terrific Broth media until $OD_{600}$ reached 0.4. The protein expression was induced by addition of 0.5 mM IPTG at 18˚C for 14-18 hrs.

$SOS^N$ expressing cells were suspended in Ni-N buffer (20 mM Tris pH 8.0, 1 M NaCl, 1 M Urea, 0.5 mM TCEP). The cells were lysed by sonication, and the insoluble fraction was separated by ultracentrifugation. The supernatant was applied to a HisTrap column (GE Healthcare), and $SOS^N$ was eluted with 400 mM Imidazole. His6-SUMO tag was cleaved off by TEV protease while dialyzing against a Ni-N2 buffer (20 mM Tris pH 8.0, 500 mM NaCl, 500 mM urea, 5 mM β-mercaptoethanol) overnight. The cleaved $SOS^N$ protein was reapplied to a HisTrap column and the flow-through was collected and concentrated on an Amicon Ultra centrifugal filter unit (Millipore). Finally, the sample was purified on a S200 16/600 (GE Healthcare) size-exclusion column equilibrated with a SEC buffer (20 mM Tris pH 8.0, 300 mM NaCl, 0.5 mM TCEP). The pooled fractions were concentrated with an Amicon Ultra centrifugal filter unit, flash-frozen in liquid nitrogen and stored at -80˚C.

$SOS^C$ expressing cells were suspended in Ni-C buffer (20 mM Tris pH 8.0, 500 mM NaCl, 500 mM urea, 0.5 % Triton, 0.5 mM TCEP) and purified on HisTrap in the same way as $SOS^N$. The eluate from the HisTrap column was dialyzed against a Ni-C2 buffer (20 mM sodium phosphate pH 6.5, 200 mM NaCl, 500 mM urea, 5 mM β-mercaptoethanol) while cleaving the tag with a TEV protease. The $SOS^C$ fragment was then reapplied to the HisTrap column and separated from the uncleaved $SOS^C$ fraction. The pooled fractions were diluted to half using a 20 mM sodium phosphate pH 6.5 buffer before applying to a HiTrap SP FF column (GE Healthcare) equilibrated with SP-A buffer (20 mM sodium phosphate pH 6.5, 100 mM NaCl, 500 mM urea, 1 mM DTT). A gradient of up to 1 M NaCl was applied and the fractions containing SOS-C were collected. The pooled fraction was flash-frozen by liquid nitrogen, and stored at -80˚C. The final yields of both $SOS^N$ and the $SOS^C$ fragments were about 2 mg per 1 L culture.

Purified $SOS^N$ and $SOS^C$ were mixed together at approximately 2 μM concentrations in an intein buffer (20 mM Tris pH 8.0, 100 mM NaCl, 5 mM TCEP) and incubated at 4˚C overnight. The ligated full-length SOS ($SOS^{FL}$) was diluted by 20 mM Tris pH 8.0 buffer to half the NaCl concentration and applied to a MonoQ column (GE Healthcare). The protein was purified on the column with MonoQ-A buffer (20 mM Tris pH 8.0, 50 mM NaCl, 0.5 mM TCEP) by applying a gradient of NaCl to 1 M. Typical yield of $SOS^{FL}$ was about 30 %. The final $SOS^{FL}$ protein contains two mutations: T1049C and M1050F, as a "scar" of the intein reaction, but otherwise the sequence is intact.

***$SOS^{catPR}$*** Rosetta (DE3) bacteria were transformed with a T7 expression vector containing the ORF, $His_6$-MBP-$(Asn)_{10}$-TEV-SOSCatPR (533–1,333 aa; C838A, C635A, C980A) derived from the SOS1 human gene. Transformed bacteria were cultured in 10 L of Terrific broth media (22711-02; Invitrogen) at 37 ˚C. After OD600 reached .7, the temperature was lowered to 18˚C for one hour and expression was induced with 0.1 M isopropyl β-D-1-thiogalactopyranoside. Cells were allowed to grow for 10 hours at 25˚C and harvested by centrifugation. Cells were resuspended in 50 mM $Na_2HPO_4$ (pH=8), 500 mM NaCl, 0.4 mM BME, 1 mM PMSF, 20 μg/mL DNase, and 10% glycerol and lysed by microfluidization. The bacterial lysate was recirculated over two 5mL HiTrap chelating columns (GE Healthcare) charged with $CoCl_2$. The HiTrap columns were extensively washed with 50 mM $Na_2HPO_4$ (pH=8), 500 mM NaCl, 0.4 mM BME before gradient elution with a buffer containing 50 mM $Na_2HPO_4$ (pH=8), 500 mM NaCl, 500mM Imidazole, 0.4 mM BME. Column eluate was dialyzed overnight into a buffer containing 50 mM $Na_2HPO_4$ (pH=8), 400 mM NaCl, and 0.4 mM BME in the presence

of .1mg/mL TEV protease to cleave the $His_6$-MBP-$(Asn)_{10}$ tag. After TEV site cleavage, Ser-Asn-Ala amino acids remain in the N-terminus of $SOS^{CatPR}$. After dialysis and tag cleavage, the protein was recirculated over a HiTrap chelating column where all his-tagged proteins are removed. The column flow-through, containing $SOS^{CatPR}$, was buffer exchanged into a buffer containing 20 mM Tris (pH=8), 50 mM NaCl, and 1 mM DTT and loaded into a MonoS cation exchange column (GE Healthcare) equilibrated with the same buffer. Bound $SOS^{CatPR}$ (pI=8.57) eluted as a single peak between 120-275mM NaCl. Column eluate was spin concentrated with a Vivaspin 10 (GE Healthcare) and loaded into a Superdex200 (GE Healthcare) gel filtration column equilibrated in 20 mM Tris (pH 8), 200 mM NaCl, 10% glycerol, and 1 mM TCEP. Fractions with high purity of $SOS^{CatPR}$ were collected and concentrated to 15 uM before freezing in liquid nitrogen and storing in -80˚C freezer.

***RBD-K65E*** BL21 (DE3) bacteria were transformed with a pETM11 expression vector containing the ORF, $his_6$-GST-PreScission-SNAPtag-Raf1 RBD (56-131 aa; K65E) derived from the Raf-1 human gene. Transformed bacteria where cultured in 3 L of Terrific broth media (22711-02; Invitrogen) at 37 ˚C. After OD600 reached .8, the temperature was lowered to 18˚C for one hour and expression was induced with 0.1 M isopropyl β-D-1-thiogalactopyranoside. Cells were allowed to grow for 15 hours at 18˚C and harvested by centrifugation. Cells were resuspended in 50 mM $Na_2HPO_4$ (pH=8), 300 mM NaCl, 0.4 mM BME, 1 mM PMSF, and 20 µg/mL DNase and lysed by microfluidization. The bacterial lysate was recirculated over a 5mL HiTrap chelating columns (GE Healthcare) charged with $CoCl_2$. The HiTrap column was extensively washed with 50 mM $Na_2HPO_4$ (pH=8), 300 mM NaCl, 0.4 mM BME before gradient elution with a buffer containing 50 mM $Na_2HPO_4$ (pH=8), 300 mM NaCl, 500mM Imidazole, 0.4 mM BME. The column eluate was dialyzed overnight into a buffer containing 50 mM $Na_2HPO_4$ (pH=8), 300 mM NaCl, and 0.4 mM BME in the presence of .1mg/mL PreScission protease to cleave the $His_6$-GST tag. After dialysis and tag cleavage, the protein was recirculated over a HiTrap chelating column where all his-tagged proteins are removed. The column flow-through, containing SNAP-RBD, was spin concentrated with a Vivaspin 10 (GE Healthcare) and loaded into a Superdex75 (GE Healthcare) gel filtration column equilibrated in 20 mM Tris (pH=8), 200 mM NaCl, 10% glycerol, and .5 mM TCEP. RBD was concentrated to 87 uM before freezing in liquid nitrogen and storing in -80˚C freezer.

***Protein labeling using maleimide*** Proteins were diluted to 100 µM (or less) with 5 mM TCEP. The proteins were then allowed to react with 1 mM Alexa Fluor 488, 555 or 647 maleimide dye for 2 hr in room temperature. The reaction was then quenched with 5 mM BME for 10 min. Excess dye was removed with multiple rounds of size exclusion chromatography (Sephadex G-25).

Functionalized supported membranes

Chromium patterns (100 nm thick and 5 nm high) were fabricated by the Pulsed Nanoimprint Lithography method (Pulsed NIL) (51) (ThunderNIL Srl, Italy). Briefly, a stamp with desired patterns was fabricated by electron beam lithography, and was treated with hydrophobic trichlorosilanes to make it non-adhesive. Pulsed NIL was performed on glass substrates, which were previously spin coated with 120 nm thick mr-l 7010 resist, using the stamp. Residual resist film on the glass substrate was etched off using

oxygen plasma before the chromium lift-off process. Nanopatterned substrates were cleaned with 2% Hallmanex III solution (Hellma Analytics) for 30 min followed by 15 min bath sonication in 1:1 IPA/$H_2O$ and $H_2O$ before piranha etching. Glass substrates (no. 1.5 thickness) were prepared by 5 min piranha etching ($H_2SO_4$:$H_2O_2$ = 3:1 by volume), followed by excessive rinsing of $H_2O$ (Milli-Q). Glass substrates were blow dried with air before depositing small unilamellar vesicles (SUVs) to form supported lipid bilayers (SLBs).

SUVs were prepared by mixing DOPC: $Ni^{2+}$-NTA-DOGS: PE MCC:$PIP_2$ lipids = 92:4:2:2 by molar percent in chloroform. If visualization of the bilayers was required, an additional 0.005% of TR-DHPE were added to the lipid composition. The solution was then evaporated using a rotary evaporator for 15 min at 40°C. Dried lipid films were further blow dried with $N_2$ for 15 min. Lipids were resuspended in $H_2O$ by vortexing, resulting in a concentration of 1 mg/mL. Finally, the vesicle solution was sonicated for 90 s in an ice-water bath to make SUVs. The membrane reconstitution system was prepared on a flow chamber (µ-Slide, Ibidi). SLBs were formed on a glass substrate by incubating the SUVs mixed with 10 mM TBS for at least 30 min. The chambers were then rinsed with TBS buffer. TBS buffer refers to 20 mM TBS buffer with 5 mM $MgCl_2$ at pH 7.4 unless stated otherwise. Next, 1 mg/mL BSA in TBS buffer was incubated for 10 min to block defects in supported membranes. After rinsing, H-Ras was incubated at 0.4 mg/mL for 2 hr 30 min in TBS buffer. 5 mM BME was then added to stop the reaction. Next, the solution was buffer exchanged into TBS buffer containing 1 mM TCEP. Proteins were centrifuged for 20 min at 4°C beforehand to remove aggregates. Hck and LAT were incubated at 4 and 63 nM, respectively, for 10 min to attach to the bilayers via his-tag – $Ni^{2+}$NTA chemistry (*29*). The system then sat for 20 min to let unstably bound membrane proteins to dissociate from the surface; during this step, 1 mM ATP and 100 µM GDP were included to phosphorylate LAT and ensure nucleotide loading in Ras. Between all incubation steps, the chambers were rinsed with TBS buffer. The fluidity of the membrane-bound proteins was examined by fluorescent recovery after photobleaching (FRAP) or single-particle tracking (SPT). Densities of membrane proteins were estimated by establishing a calibration curve between epifluorescence average intensity and densities measured by fluorescence correlation spectroscopy (FCS) (FCS methods were described previously (*31*)). All preparations were done at room temperature unless stated otherwise.

Microscopy

TIRF experiments were performed on a motorized inverted microscope (Nikon Eclipse Ti-E; Technical Instruments, Burlingame, CA) equipped with a motorized Epi/TIRF illuminator, motorized Intensilight mercury lamp (Nikon C-HGFIE), Perfect Focus system, and a motorized stage (Applied Scientific Instrumentation MS-2000, Eugene, OR). A laser launch with 561 and 640 nm (Coherent OBIS, Santa Clara, CA) diode lasers was controlled by an OBIS Scientific Remote (Coherent Inc., Santa Clara, CA) and aligned into a fiber launch custom built by Solamere Technology Group, Inc. (Salt Lake City, UT). The optical path was then aligned to a 100x 1.49 NA oil immersion TIRF objective (Nikon). A dichroic beamsplitter (ZT405/488/561/640rpc; Chroma Technology Corp., Bellows Falls, VT) reflected the laser light through the objective lens and fluorescence images were recorded using an EM-CCD (iXon 897DU; Andor Inc.,

South Windsor, CT) after passing through a laser-blocking filter (ZET405/488/561/640m-TRF; Chroma Technology Corp., Bellows Falls, VT). Laser powers measured at the sample were approximately 2.7 mW and 0.7 mW for 561 nm and 647 nm, respectively. Exposure times were set to 40 ms and 20 ms for 561 nm and 647 nm, respectively. All acquisitions were obtained using Micro-Manager (53). A TTL signal from the appropriate laser triggered the camera exposure.

Imaging of SOS and RBD

All imaging experiments were performed in imaging buffer consisted of 2 mM UV-treated trolox, 10 mM βME, 20 mM glucose, 320 μg/mL glucose oxidase, 50 μg/mL catalase (52) and 0.01 mg/mL Casein in TBS buffer. To trigger SOS recruitment, ~1 nM $SOS^{FL}$-Alexa Fluor 555, 20 nM Grb2, 10 nM RBD-K65E-Alexa Fluor 647, and 120 μM GTP were added into solution with the imaging buffer. This set of conditions will result mostly in either one or zero SOS recruited per corral during a 10-min imaging session. We performed the corral assay at a very dilute $SOS^{FL}$ concentration (~ 1 nM), such that at any given time, only about ~ 3% of the corrals were occupied with a SOS molecule (accounting for its labeling efficiency). Therefore, the probability of two SOS molecules localized to the same corral at a given time is < 0.1% (estimated with Poisson statistics).

In our experiments, spectral bleed-through is minimal since both 561 and 647 dyes are on proteins with very low densities (unlike conventional bulk colocalization experiments). SOS channel is strictly at the single-molecule level (averaged density < 0.05 $\mu m^{-2}$); initial accumulation of RBD (at the timescale that activation time of SOS is measured) has very little detectable signals in the 561 channel (Fig. 1D, S3).

Time-lapse acquisition was taken at a framerate of 0.5 Hz with a very low power (~2.7 mW for 561 before the objection). This acquisition strategy allows long visualization (> 100 s) of SOS localization by lowering the photobleaching rates (bleaching time was ~130 sec with imaging buffers); bleaching rate was estimated from immobilized SOS on glass substrates.

The analysis was performed on the central square of 300×300 pixel to decrease uneven illumination. Further processing corrected the remaining uneven illumination in the region of interest: the time-lapse images were background-subtracted and field illumination corrected in Fiji; Stage drift was corrected using the 'Image Stabilizer' FIJI plugin (54). Intensity profiles for individual corrals were extracted and further analyzed with a custom script in Matlab 2016.

***Statistics*** A typical set of experiments (on a single day) involves 6-12 independent supported membrane microarray chips, each of which have ≥ 2,000 experimentally resolvable membrane corrals (partially shown in Fig. 1). From the ~2,000 corrals imaged in each experiment, ~ 200 single-molecule observations/trajectories were collected (Fig. 1D, E) with the remaining ~1800 corrlas providing robust background measurement as well as providing controls for spatial variation in the sample or other sources of error (Fig. S3D). This collected data was used to construct the histograms (Fig. 2, 3). Then, the full set of experiments were repeated independently on a different day for a minimum of 3 additional iterations; experiments with the PR domains (Fig. 4) were repeated 3 times. To benchmark the assay between different days, we repeated the condition of Grb2-mediated full-length SOS activation as a standard (≥ 10 fully independent iterations).

Activation time analysis

Trajectory analyses were performed with Matlab 2016, after preprocessing from Fiji. The intensities of SOS and RBD channels were plotted after smoothing with average filtering of 5 and 7 data points, respectively. The change points of each channel were analyzed with the "findchangepts" function in Matlab. For SOS channel, a change point was detected when the mean changed; for RBD channel, a change point was detected when the slope (i.e. rate of RasGTP production) changed. The threshold used depends on the mean and noise of the intensities. The performance of the thresholds used was benchmarked with corrals without SOS recruitment (Fig. S3D) and corrals with SOS activation (Fig. 1D). In our application, we found a threshold of 12,000 and 20,000 worked well for strict change-point detection of SOS and RBD, respectively. The activation time $t_{act}$ for each trajectory was then evaluated as such:

$$t_{act} = \tau_{RasGTP} - \tau_{SOS}$$

if the RBD channel has a change point while SOS is recruited Eq. [S1]

where $\tau_i$ denotes the time of the first change point. For the rejection time $t_{rej}$, it is calculated as:

$$t_{rej} = \tau'_{SOS} - \tau_{SOS}$$

if the RBD channel has no change point before SOS dissociates Eq. [S2]

where $\tau'$ denotes the second change point, or dissociation from membranes. The rejection time is the dwell times of SOS given that no activation occurs. Corrals without recruited SOS were discarded from the analysis. In some rare trajectories, a corral can have two SOS on membranes (roughly doubling the intensities) at the same time; these trajectories were also filtered from the analysis. A representative analysis of interpretable SOS and RBD trajectories are shown in Fig. 1D, E and S3.

***Spontaneous activation of SOS*** SOS is primarily shuttled onto membranes by Grb2. In the absence of Grb2, SOS can, in rare cases, temporarily escape from autoinhibition and recruit to membranes through binding Ras at its allosteric pocket. This receptor-independent activation is characterized to have an exponential activation time distribution (Fig. 3). This activation pathway contributes, though minorly (~10%), to SOS activation even under the presence of Grb2. To quantify the activation time distribution for Grb2-mediated pathway, we subtracted the estimated receptor-independent contribution from the activation time histogram of $SOS^{FL}$ activation with Grb2. Receptor-independent activation contributes less in the case of $SOS^{catPR}$ activation since the lack of N-terminal autoinhibition causes Grb2-mediated recruitment of $SOS^{catPR}$ to increase by 3-fold compared to $SOS^{FL}$; therefore, we did not subtract the receptor-independent count in this case.

***Goodness-of-fit analysis for Fig. 3*** The following table shows the reduced chi-squared analysis of Fig. 3F-I between $N = 1$ intermediate and exponential kinetics ($N = 0$). The model (Fig. 3A-D) is supported with lower reduced chi-squared statistics,

although only marginally in the case without $PIP_2$. Therefore, we further analyze the goodness-of-fit for the proofreading ratio, $p_{rej}/p_{act}$, for the case without $PIP_2$. Comparing the prediction of model with the data, the residual sum of squares for $N = 0$ and $N = 1$ are $1.03 \times 10^3$ and $5.83 \times 10^2$, respectively. Therefore, $N = 1$ describes the case without PIP2 better over $N = 0$.

| *Model* | $SOS^{FL}$ | *w/o Grb2* | $SOS^{catPR}$ | *w/o* $PIP_2$ |
|---|---|---|---|---|
| $N = 0$ | $8.6 \times 10^{-7}$ | $9.1 \times 10^{-7}$ | $2.1 \times 10^{-7}$ | $1.304 \times 10^{-7}$ |
| $N = 1$ | $2.5 \times 10^{-7}$ | $10.2 \times 10^{-7}$ | $5.2 \times 10^{-7}$ | $1.298 \times 10^{-7}$ |

Dwell time analysis

Single molecules were tracked with a customized program written in Igor (*10*). The analysis was performed on the central 350×350 pixel region of the images to minimize uneven illumination. The dwell times from each binding event were sorted into a histogram with the frame interval as the bin. The histogram was normalized and fitted to a probability distribution of multi-exponential kinetics:

$$p(t) = \sum_{i=1}^{N} \alpha_i k_i e^{-k_i t} \qquad \text{Eq. [S3]}$$

where $N$ is the number of population, $\alpha_i$ is the fraction of the population $i$ and $k_i$ is the rate constant for the population $i$. A typical histogram consisted of 2,000-5,000 data points. Fitting procedure initiated with a single exponential. In cases of poor fitting, a maximum of two populations was used.

Step-size distribution analysis

Single-molecule were tracked with a customized program written in Igor (*10*). The analysis was performed on the central 350×350 pixel region of the images to minimize uneven illumination. The step size between each frame was sorted into a histogram with a bin of 0.02 μm. The histogram was normalized and fitted to a probability distribution of a single or double freely diffusive population:

$$p(r) = \sum_{i=1}^{N} \alpha_i \frac{r}{2D_i \Delta t} e^{-\frac{r^2}{4D_i \Delta t}} \qquad \text{Eq. [S4]}$$

where $N$ is the number of population, $\alpha_i$ is the fraction of the population $i$ and $D_i$ is the diffusion coefficient for the population $i$. Immobilized particles were filtered from the analysis.

Activation kinetics of SOS

In the following, we derive the activation time and rejection time distribution for a simple model of SOS activation (*10*). For a cytosolic enzyme to activate on membrane surfaces at time $t$, it must satisfy two conditions: ***i***) the enzyme reaches the activation state at time $t$, and ***ii***) the enzyme remains bound to the membrane. This molecular description leads to a probabilistic statement of the activation time distribution $p_{act}(t)$:

$$p_{act}(t) = p_N(t) P(t < T_D) = p_N(t) \cdot e^{-k_{-1} t} \qquad \text{[S5]}$$

where $t$ is the time, $T_D$ is the random variable for the time to dissociate from membranes, $p_N(t)$ is the distribution of the activation kinetics, and $P$ denotes the cumulative probability. The dissociation of a molecule from membranes is assumed to be a Poisson process with a rate constant $k_{-1}$. Considering the simplifying case where the individual kinetic intermediates have equal rate constants, $p_N(t) = k_N^{N+1} t^N e^{-k_N t}/N!$ where $N$ is the number of kinetic intermediates each with a transition rate constant $k_N$. This simplification is particularly a good approximation where the intermediate(s) are well-resolved in the experimental timescale. For the rejection time distribution, $p_{rec}(t)$ can be expressed in a similar argument:

$$p_{rej}(t) = P(t < T_N)p_D(t) = \int_t^\infty p_N(t')dt' \cdot k_{-1}e^{-k_{-1}t} = \frac{\Gamma(N,t)}{N!} \cdot k_{-1}e^{-k_{-1}t} \quad [S6]$$

where $T_N$ is the random variable for the time to activate on membranes, $p_D(t)$ is the distribution of dissociation, and $\Gamma(N,t) = \int_{k_N t}^\infty t'^N e^{-t'} dt'$, which is the upper incomplete gamma function. Note that in our definition, the probability of activation, $P_{act}$, can be easily obtained by $P_{act} = \int_0^\infty p_{act}(t)dt$; a similar expression also defines the probability of rejection, $P_{rej} = \int_0^\infty p_{rej}(t)dt$, such that $P_{act} + P_{rej} = 1$.

***Fig. 4 parameter definition*** The fold-increase of SOS activity is defined as $x_{sos} = \frac{P_{act,activated} - P_{act,basal}}{P_{act,basal}}$, where the probability of activation is calculated following the previous equations. The basal state refers to the unassembled, monovalent SOS interaction with LAT via Grb2.

**Supplementary Text**

Turnover of pY on LAT

An interesting feature of the LAT assembly indeed is the individual molecular binding events can turn over much more rapidly than the assembly itself evolves (*10, 12*). Although it is assumed that competing kinase and phosphatase reactions may lead to constant turnover of pY on LAT, little is actually known about this at present. However, it is clear that, during T-cell receptor signaling, LAT forms stable macroscopic assemblies with Grb2 and SOS (*7*). In addition, the study by Su *et al.* (*11*) shows that phosphatases can be excluded in these LAT assemblies, suggesting that the turnover of pY is slower within LAT assembly. In any case, the prominent driving force for LAT assembly is the substantially enhanced local kinase activity around LAT assembly during T-cell receptor triggering – this results in stable long-lived LAT assemblies, which may or may not experience pY turnover internally. Ultimately it is the LAT organization, not the turnover of pY, that defines its properties and our reconstitutions measure SOS activity vs. LAT organization.

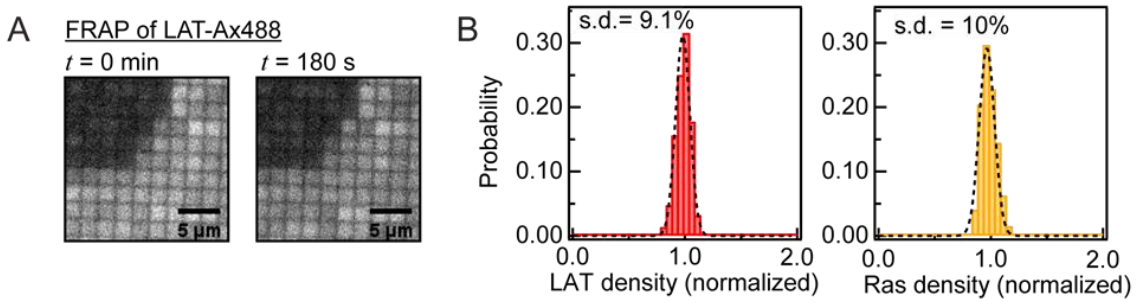


**Fig. S1.**

Characterization of the supported membrane microarray. (A) Fluorescence recovery after photobleaching (FRAP) of membrane-bound LAT proteins in the supported membrane corrals. Membrane-associated proteins were restricted within each corral. (B) Intensities of LAT-Alexa Fluor 488 and RasGTP (measured by RBD-Alexa Fluor 647 after full activation by SOS) across different corrals. The dashed lines are fitting to a Gaussian distribution. S.d., standard deviation. Both LAT and Ras had small density variations across the membrane microarray in our experiments.

| | $SOS^{FL}$ | $SOS^{catPR}$ | Grb2 | $PIP_2$ |
|---|---|---|---|---|
| Receptor-mediated activation | + | - | + | + |
| Receptor-independent activation | + | - | - | + |
| Loss of autoinhibition | - | + | + | + |
| Slower release of autoinhibition | + | - | + | - |

**Fig. S2**

Experimental design for the data in Fig. 3.

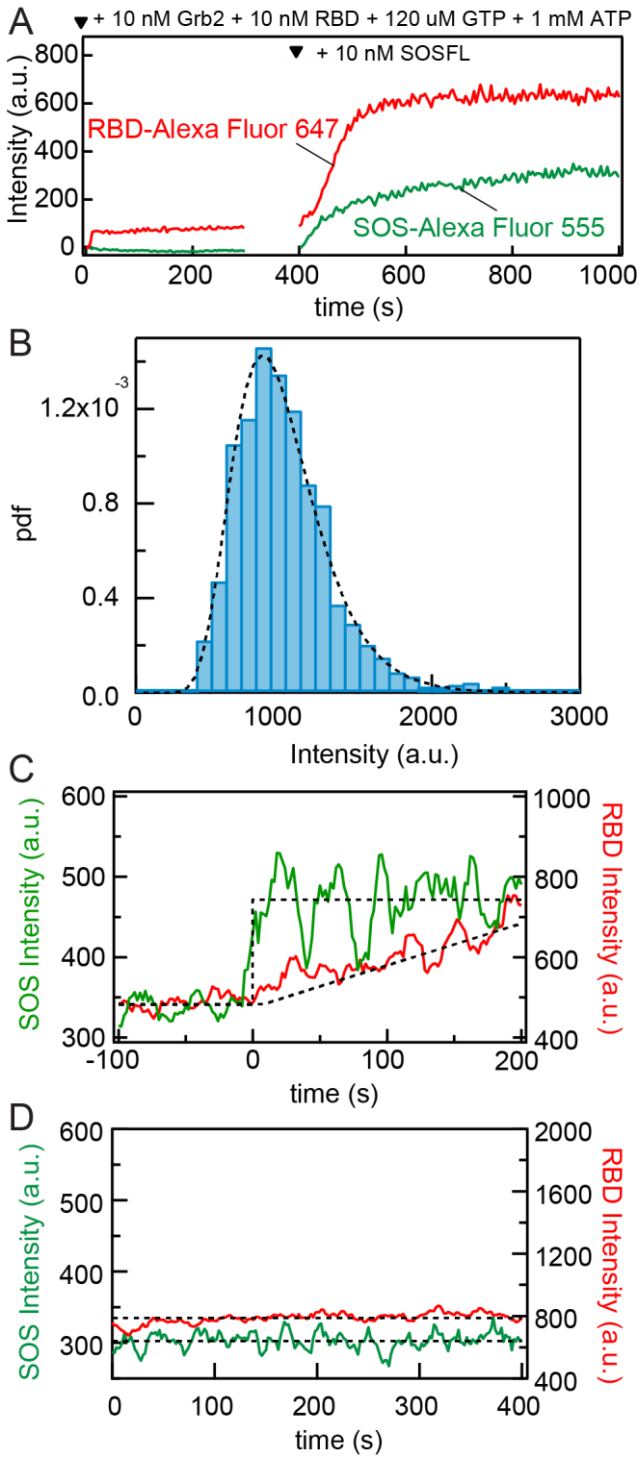


**Fig. S3**

Characterization of the single-molecule SOS activation assay. (A) Intensities of $SOS^{FL}$-Alexa Fluor 555 and RBD-K65E-Alexa Fluor 647 on unrestricted supported membranes with Ras, LAT and Src kinase Hck. The addition of $SOS^{FL}$ catalyzed Ras loading with GTP, thus triggered RBD recruitment onto the membrane. This bulk experiment demonstrates that the RBD used in our reconstitution binds specifically to RasGTP. (B)

Single-molecule intensity distribution of $SOS^{FL}$-Alexa Fluor 555. The histogram is fitted to a log-normal distribution, which corresponds to the intensity distribution of a single fluorophore. (C) An example of SOS activation without Grb2. In this trajectory, the time from SOS recruitment onto the membrane to activation was near instantaneous; the activation time was around the resolution limit of the assay. (D) An example of corral without SOS recruitment. These trajectories were also used to benchmark the performance of the analysis.

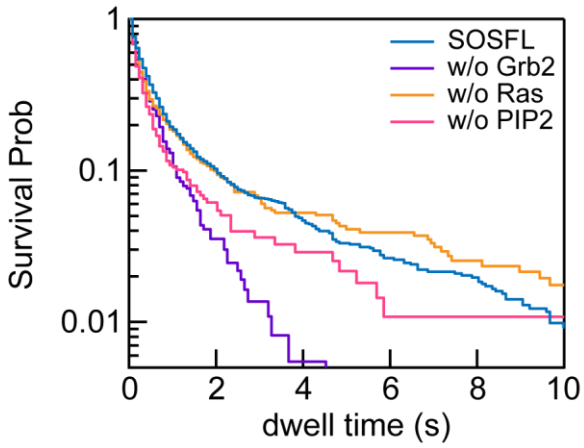


| | $SOS^{FL}$ | w/o Grb2 | w/o Ras | w/o $PIP_2$ |
|---|---|---|---|---|
| $SOS^{FL}$ | + | + | + | + |
| Grb2 | + | - | + | + |
| Ras | + | + | - | + |
| $PIP_2$ | + | + | + | - |

**Fig. S4**

SOS dwell time is primarily mediated by Grb2. Single-molecule dwell time analysis of $SOS^{FL}$-Alexa Fluor 555 with or without Grb2, Ras, or PIP2. All single-molecule tracking experiments (Fig. S4-6) were performed with GDP in the solution, mimicking the onset of SOS recruitment in response to receptor activation. The long dwelling species of SOS (>1 s) is mostly modulated by Grb2 (without Grb2, SOS dwells shorter on the membrane). The single-molecule tracking experiments were obtained by continuous stream acquisition (with a framerate of 21 Hz). Therefore, photobleaching was higher such that the apparent SOS dwell times were shorter than those measured from the SOS activation assay.

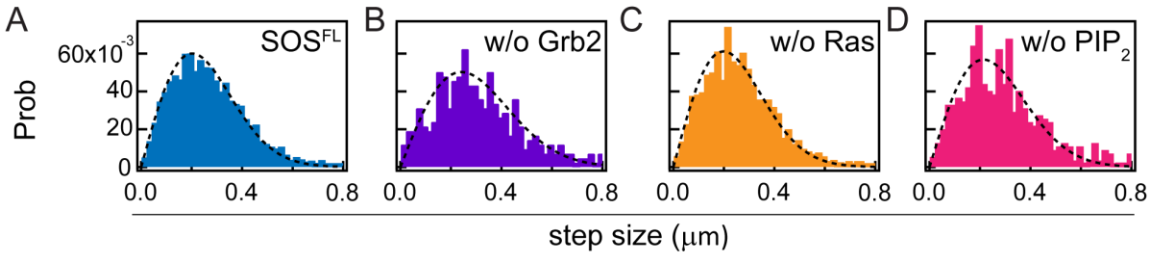


E

| | SOS$^{FL}$ | w/o Grb2 | w/o Ras | w/o $PIP_2$ |
|---|---|---|---|---|
| SOS$^{FL}$ | + | + | + | + |
| Grb2 | + | - | + | + |
| Ras | + | + | - | + |
| $PIP_2$ | + | + | + | - |
| Single Particle Tracking of SOS$^{FL}$ | | | | |
| D ($\mu m^2/s$) | 0.26 | 0.37 | 0.26 | 0.29 |

**Fig. S5**

Initial membrane engagement of SOS is modulated by Grb2. (A to D) Step-size distributions of SOS$^{FL}$-Alexa Fluor 555 from single-molecule tracking (SMT) analysis. The time intervals between acquisitions were 0.078 s. Any immobile SOS (typically with a fraction < 20%) were filtered during the analysis. Since the mobility of membrane-associating protein (SOS in this case) is typically determined by its interactions with membrane components (LAT, Ras or PIP2), the diffusion analysis indicates that the initial membrane engagement state of SOS is primarily mediated by Grb2 (without Grb2, SOS diffuses faster).

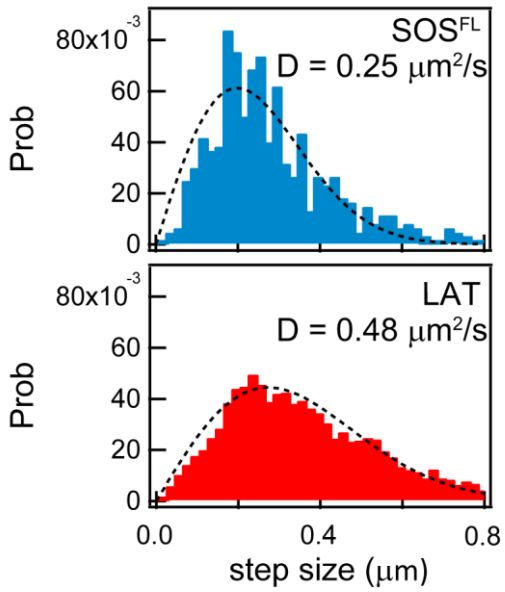


**Fig. S6**

Multivalent interactions of LAT:Grb2:SOS. Step-size distributions of $SOS^{FL}$-Alexa Fluor 555 and LAT-Alexa Fluor 555 from single-molecule tracking (SMT) analysis. LAT and SOS were measured in different but duplicated samples, and acquired under identical imaging condition in the same day. The time intervals between acquisitions were 0.078 s. On the membrane, the mobility of membrane-associating proteins is mostly determined by its interactions with membrane components due to viscosity (LAT were chelated to $Ni^{2+}$-NTA-DOGS). Therefore, the mobility of SOS indicates the number of interacting LAT molecules (although the relationship is not necessarily linear). The slower mobility of SOS compared to freely diffusing LAT suggests that membrane-recruited SOS interacts with at least two LAT molecules on the membrane. $PIP_2$-bound SOS is rare on this timescale (~sec) since PIP2-mediated autoinhibition release takes 10-100 sec.

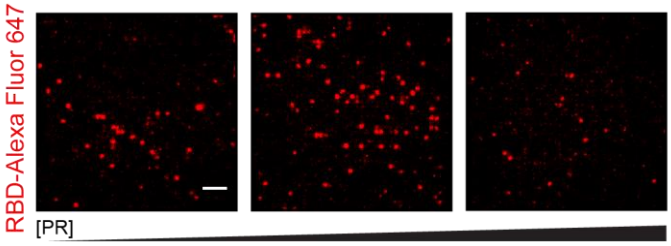


**Fig. S7**

The competing effect of the PR domains on SOS activation. These experiments were similar to ones in Fig. 4. Images were taken at 15 min after the addition of $SOS^{FL}$. The PR domains compete with $SOS^{FL}$ to recruit onto the membrane. However, at intermediate PR concentrations (50 nM) (the middle image), Ras activation was promoted by the PR domains, suggesting a non-trivial enhancement of SOS activation from LAT assemblies. At higher PR concentrations (> 100 nM), this enhancement was abolished, primarily due to $SOS^{FL}$ outcompleted by the PR domains. Scale bar, 5 μm.

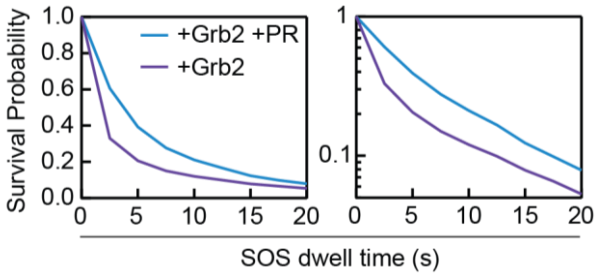


**Fig. S8**

Single-molecule dwell time analysis of $SOS^{FL}$-Alexa Flour 555 with or without the PR domains.

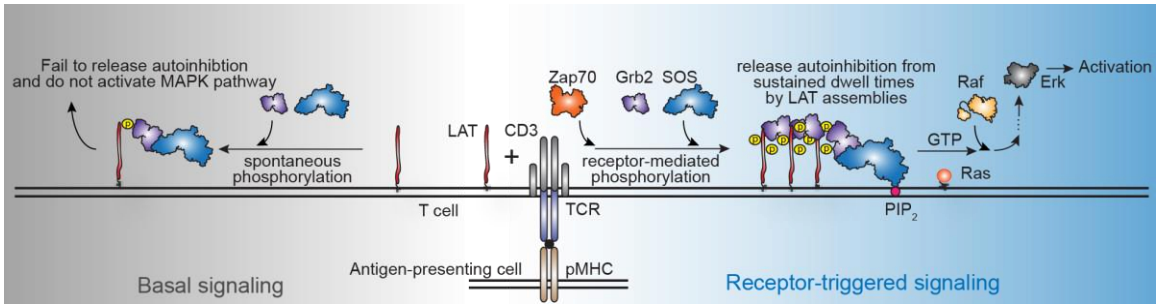


**Fig. S9**

The signaling benefit of kinetic proofreading in SOS activation. With kinetic proofreading, the signaling system can differentiate receptor-mediated SOS recruitments from spontaneous SOS localizations by membrane dwell times. In this scenario, the activation of the MAPK pathway depends on the dynamical identity of SOS, in additional to the number of membrane recruitments.

**Movie S1**

Single-molecule SOS activation assay. An example of simultaneous imaging of $SOS^{FL}$-Alexa Fluor 555 (green channel) and RBD-K65E-Alexa Fluor 647 (red channel) in the supported membranes microarray. $SOS^{FL}$, Grb2 and GTP were injected at time 0. Scale bar, 10 μm.

**References and Notes**


1. L. E. Samelson, Signal transduction mediated by the T cell antigen receptor: The role of adapter proteins. *Annu. Rev. Immunol.* **20**, 371–394 (2002). doi:10.1146/annurev.immunol.20.092601.111357 Medline

2. J. Schlessinger, Cell signaling by receptor tyrosine kinases. *Cell* **103**, 211–225 (2000). doi:10.1016/S0092-8674(00)00114-8 Medline

3. H. Sondermann, S. M. Soisson, S. Boykevisch, S.-S. Yang, D. Bar-Sagi, J. Kuriyan, Structural analysis of autoinhibition in the Ras activator Son of sevenless. *Cell* **119**, 393–405 (2004). doi:10.1016/j.cell.2004.10.005 Medline

4. N. W. Gale, S. Kaplan, E. J. Lowenstein, J. Schlessinger, D. Bar-Sagi, Grb2 mediates the EGF-dependent activation of guanine nucleotide exchange on Ras. *Nature* **363**, 88–92 (1993). doi:10.1038/363088a0 Medline

5. P. Bandaru, Y. Kondo, J. Kuriyan, The interdependent activation of Son-of-Sevenless and Ras. *Cold Spring Harb. Perspect. Med.* **9**, a031534 (2019). doi:10.1101/cshperspect.a031534 Medline

6. T. Shi, M. Niepel, J. E. McDermott, Y. Gao, C. D. Nicora, W. B. Chrisler, L. M. Markillie, V. A. Petyuk, R. D. Smith, K. D. Rodland, P. K. Sorger, W.-J. Qian, H. S. Wiley, Conservation of protein abundance patterns reveals the regulatory architecture of the EGFR-MAPK pathway. *Sci. Signal.* **9**, rs6 (2016). doi:10.1126/scisignal.aaf0891 Medline

7. J. C. D. Houtman, H. Yamaguchi, M. Barda-Saad, A. Braiman, B. Bowden, E. Appella, P. Schuck, L. E. Samelson, Oligomerization of signaling complexes by the multipoint binding of GRB2 to both LAT and SOS1. *Nat. Struct. Mol. Biol.* **13**, 798–805 (2006). doi:10.1038/nsmb1133 Medline

8. R. L. Kortum, L. Balagopalan, C. P. Alexander, J. Garcia, J. M. Pinski, R. K. Merrill, P. H. Nguyen, W. Li, I. Agarwal, I. O. Akpan, C. L. Sommers, L. E. Samelson, The ability of Sos1 to oligomerize the adaptor protein LAT is separable from its guanine nucleotide exchange activity in vivo. *Sci. Signal.* **6**, ra99 (2013). doi:10.1126/scisignal.2004494 Medline

9. A. Nag, M. I. Monine, J. R. Faeder, B. Goldstein, Aggregation of membrane proteins by cytosolic cross-linkers: Theory and simulation of the LAT-Grb2-SOS1 system. *Biophys. J.* **96**, 2604–2623 (2009). doi:10.1016/j.bpj.2009.01.019 Medline

10. W. Y. C. Huang, Q. Yan, W.-C. Lin, J. K. Chung, S. D. Hansen, S. M. Christensen, H.-L. Tu, J. Kuriyan, J. T. Groves, Phosphotyrosine-mediated LAT assembly on membranes drives kinetic bifurcation in recruitment dynamics of the Ras activator SOS. *Proc. Natl. Acad. Sci. U.S.A.* **113**, 8218–8223 (2016). doi:10.1073/pnas.1602602113 Medline

11. X. Su, J. A. Ditlev, E. Hui, W. Xing, S. Banjade, J. Okrut, D. S. King, J. Taunton, M. K. Rosen, R. D. Vale, Phase separation of signaling molecules promotes T cell receptor signal transduction. *Science* **352**, 595–599 (2016). doi:10.1126/science.aad9964 Medline

12. W. Y. C. Huang, H. K. Chiang, J. T. Groves, Dynamic scaling analysis of molecular motion within the LAT:Grb2:SOS protein network on membranes. *Biophys. J.* **113**, 1807–1813 (2017). doi:10.1016/j.bpj.2017.08.024 Medline

13. W. Y. C. Huang, J. A. Ditlev, H. K. Chiang, M. K. Rosen, J. T. Groves, Allosteric modulation of Grb2 recruitment to the intrinsically disordered scaffold protein, LAT, by remote site phosphorylation. *J. Am. Chem. Soc.* **139**, 18009–18015 (2017). doi:10.1021/jacs.7b09387 Medline

14. B. J. Mayer, J. Yu, Protein clusters in phosphotyrosine signal transduction. *J. Mol. Biol.* **430**, 4547–4556 (2018). doi:10.1016/j.jmb.2018.05.040 Medline

15. S. Banjade, M. K. Rosen, Phase transitions of multivalent proteins can promote clustering of membrane receptors. *eLife* **3**, e04123 (2014). doi:10.7554/eLife.04123 Medline

16. L. Iversen, H.-L. Tu, W.-C. Lin, S. M. Christensen, S. M. Abel, J. Iwig, H.-J. Wu, J. Gureasko, C. Rhodes, R. S. Petit, S. D. Hansen, P. Thill, C.-H. Yu, D. Stamou, A. K. Chakraborty, J. Kuriyan, J. T. Groves, Ras activation by SOS: Allosteric regulation by altered fluctuation dynamics. *Science* **345**, 50–54 (2014). doi:10.1126/science.1250373 Medline

17. J. T. Groves, N. Ulman, S. G. Boxer, Micropatterning fluid lipid bilayers on solid supports. *Science* **275**, 651–653 (1997). doi:10.1126/science.275.5300.651 Medline

18. J. J. Hopfield, Kinetic proofreading: A new mechanism for reducing errors in biosynthetic processes requiring high specificity. *Proc. Natl. Acad. Sci. U.S.A.* **71**, 4135–4139 (1974). doi:10.1073/pnas.71.10.4135 Medline

19. Y. K. Lee, S. T. Low-Nam, J. K. Chung, S. D. Hansen, H. Y. M. Lam, S. Alvarez, J. T. Groves, Mechanism of SOS PR-domain autoinhibition revealed by single-molecule assays on native protein from lysate. *Nat. Commun.* **8**, 15061 (2017). doi:10.1038/ncomms15061 Medline

20. S. M. Christensen, H.-L. Tu, J. E. Jun, S. Alvarez, M. G. Triplet, J. S. Iwig, K. K. Yadav, D. Bar-Sagi, J. P. Roose, J. T. Groves, One-way membrane trafficking of SOS in receptor-triggered Ras activation. *Nat. Struct. Mol. Biol.* **23**, 838–846 (2016). doi:10.1038/nsmb.3275 Medline

21. J. Gureasko, O. Kuchment, D. L. Makino, H. Sondermann, D. Bar-Sagi, J. Kuriyan, Role of the histone domain in the autoinhibition and activation of the Ras activator Son of Sevenless. *Proc. Natl. Acad. Sci. U.S.A.* **107**, 3430–3435 (2010). doi:10.1073/pnas.0913915107 Medline

22. J. T. Groves, J. Kuriyan, Molecular mechanisms in signal transduction at the membrane. *Nat. Struct. Mol. Biol.* **17**, 659–665 (2010). doi:10.1038/nsmb.1844 Medline

23. J. Gureasko, W. J. Galush, S. Boykevisch, H. Sondermann, D. Bar-Sagi, J. T. Groves, J. Kuriyan, Membrane-dependent signal integration by the Ras activator Son of sevenless. *Nat. Struct. Mol. Biol.* **15**, 452–461 (2008). doi:10.1038/nsmb.1418 Medline

24. K. K. Yadav, D. Bar-Sagi, Allosteric gating of Son of sevenless activity by the histone domain. *Proc. Natl. Acad. Sci. U.S.A.* **107**, 3436–3440 (2010). doi:10.1073/pnas.0914315107 Medline

25. M. Tartaglia, L. A. Pennacchio, C. Zhao, K. K. Yadav, V. Fodale, A. Sarkozy, B. Pandit, K. Oishi, S. Martinelli, W. Schackwitz, A. Ustaszewska, J. Martin, J. Bristow, C. Carta, F. Lepri, C. Neri, I. Vasta, K. Gibson, C. J. Curry, J. P. L. Siguero, M. C. Digilio, G.

Zampino, B. Dallapiccola, D. Bar-Sagi, B. D. Gelb, Gain-of-function SOS1 mutations cause a distinctive form of Noonan syndrome. *Nat. Genet.* **39**, 75–79 (2007). doi:10.1038/ng1939 Medline

26. J. C. D. Houtman, Y. Higashimoto, N. Dimasi, S. Cho, H. Yamaguchi, B. Bowden, C. Regan, E. L. Malchiodi, R. Mariuzza, P. Schuck, E. Appella, L. E. Samelson, Binding specificity of multiprotein signaling complexes is determined by both cooperative interactions and affinity preferences. *Biochemistry* **43**, 4170–4178 (2004). doi:10.1021/bi0357311 Medline

27. C. Zhao, G. Du, K. Skowronek, M. A. Frohman, D. Bar-Sagi, Phospholipase D2-generated phosphatidic acid couples EGFR stimulation to Ras activation by Sos. *Nat. Cell Biol.* **9**, 707–712 (2007). doi:10.1038/ncb1594 Medline

28. S. M. Margarit, H. Sondermann, B. E. Hall, B. Nagar, A. Hoelz, M. Pirruccello, D. Bar-Sagi, J. Kuriyan, Structural evidence for feedback activation by Ras.GTP of the Ras-specific nucleotide exchange factor SOS. *Cell* **112**, 685–695 (2003). doi:10.1016/S0092-8674(03)00149-1 Medline

29. J. A. Nye, J. T. Groves, Kinetic control of histidine-tagged protein surface density on supported lipid bilayers. *Langmuir* **24**, 4145–4149 (2008). doi:10.1021/la703788h Medline

30. N. H. Shah, Q. Wang, Q. Yan, D. Karandur, T. A. Kadlecek, I. R. Fallahee, W. P. Russ, R. Ranganathan, A. Weiss, J. Kuriyan, An electrostatic selection mechanism controls sequential kinase signaling downstream of the T cell receptor. *eLife* **5**, e20105 (2016). doi:10.7554/eLife.20105 Medline

31. W. C. Lin, L. Iversen, H.-L. Tu, C. Rhodes, S. M. Christensen, J. S. Iwig, S. D. Hansen, W. Y. C. Huang, J. T. Groves, H-Ras forms dimers on membrane surfaces via a protein-protein interface. *Proc. Natl. Acad. Sci. U.S.A.* **111**, 2996–3001 (2014). doi:10.1073/pnas.1321155111 Medline

32. D. J. Williamson, D. M. Owen, J. Rossy, A. Magenau, M. Wehrmann, J. J. Gooding, K. Gaus, Pre-existing clusters of the adaptor Lat do not participate in early T cell signaling events. *Nat. Immunol.* **12**, 655–662 (2011). doi:10.1038/ni.2049 Medline

33. T. Gurry, O. Kahramanoğullari, R. G. Endres, Biophysical mechanism for ras-nanocluster formation and signaling in plasma membrane. *PLOS ONE* **4**, e6148 (2009). doi:10.1371/journal.pone.0006148 Medline

34. K. J. Cho, J. F. Hancock, Ras nanoclusters. *Small GTPases* **4**, 57–60 (2013). doi:10.4161/sgtp.23145 Medline

35. A. J. Stevens, Z. Z. Brown, N. H. Shah, G. Sekar, D. Cowburn, T. W. Muir, Design of a split intein with exceptional protein splicing activity. *J. Am. Chem. Soc.* **138**, 2162–2165 (2016). doi:10.1021/jacs.5b13528 Medline

36. C. B. McDonald, J. E. Balke, V. Bhat, D. C. Mikles, B. J. Deegan, K. L. Seldeen, A. Farooq, Multivalent binding and facilitated diffusion account for the formation of the Grb2-Sos1 signaling complex in a cooperative manner. *Biochemistry* **51**, 2122–2135 (2012). doi:10.1021/bi3000534 Medline

37. B. K. Jaitner, J. Becker, T. Linnemann, C. Herrmann, A. Wittinghofer, C. Block, Discrimination of amino acids mediating Ras binding from noninteracting residues affecting Raf activation by double mutant analysis. *J. Biol. Chem.* **272**, 29927–29933 (1997). doi:10.1074/jbc.272.47.29927 Medline

38. J. R. Moffitt, Y. R. Chemla, C. Bustamante, Methods in statistical kinetics. *Methods Enzymol.* **475**, 221–257 (2010). doi:10.1016/S0076-6879(10)75010-2 Medline

39. S. C. Kou, B. J. Cherayil, W. Min, B. P. English, X. S. Xie, Single-molecule Michaelis-Menten equations. *J. Phys. Chem. B* **109**, 19068–19081 (2005). doi:10.1021/jp051490q Medline

40. J. Lin, A. Weiss, Identification of the minimal tyrosine residues required for linker for activation of T cell function. *J. Biol. Chem.* **276**, 29588–29595 (2001). doi:10.1074/jbc.M102221200 Medline

41. T. W. McKeithan, Kinetic proofreading in T-cell receptor signal transduction. *Proc. Natl. Acad. Sci. U.S.A.* **92**, 5042–5046 (1995). doi:10.1073/pnas.92.11.5042 Medline

42. M. Turner, D. D. Billadeau, VAV proteins as signal integrators for multi-subunit immune-recognition receptors. *Nat. Rev. Immunol.* **2**, 476–486 (2002). doi:10.1038/nri840 Medline

43. R. E. Cutler Jr., R. M. Stephens, M. R. Saracino, D. K. Morrison, Autoregulation of the Raf-1 serine/threonine kinase. *Proc. Natl. Acad. Sci. U.S.A.* **95**, 9214–9219 (1998). doi:10.1073/pnas.95.16.9214 Medline

44. B. P. Ziemba, J. Li, K. E. Landgraf, J. D. Knight, G. A. Voth, J. J. Falke, Single-molecule studies reveal a hidden key step in the activation mechanism of membrane-bound protein kinase C-α. *Biochemistry* **53**, 1697–1713 (2014). doi:10.1021/bi4016082 Medline

45. O. Vadas, J. E. Burke, X. Zhang, A. Berndt, R. L. Williams, Structural basis for activation and inhibition of class I phosphoinositide 3-kinases. *Sci. Signal.* **4**, re2 (2011). doi:10.1126/scisignal.2002165 Medline

46. A. H. Andreotti, P. L. Schwartzberg, R. E. Joseph, L. J. Berg, T-cell signaling regulated by the Tec family kinase, Itk. *Cold Spring Harb. Perspect. Biol.* **2**, a002287 (2010). doi:10.1101/cshperspect.a002287 Medline

47. L. B. Case, X. Zhang, J. A. Ditlev, M. K. Rosen, Stoichiometry controls activity of phase-separated clusters of actin signaling proteins. *Science* **363**, 1093–1097 (2019). doi:10.1126/science.aau6313

48. Q. Yan, T. Barros, P. R. Visperas, S. Deindl, T. A. Kadlecek, A. Weiss, J. Kuriyan, Structural basis for activation of ZAP-70 by phosphorylation of the SH2-kinase linker. *Mol. Cell. Biol.* **33**, 2188–2201 (2013). doi:10.1128/MCB.01637-12 Medline

49. J. DelProposto, C. Y. Majmudar, J. L. Smith, W. C. Brown, Mocr: A novel fusion tag for enhancing solubility that is compatible with structural biology applications. *Protein Expr. Purif.* **63**, 40–49 (2009). doi:10.1016/j.pep.2008.08.011 Medline

50. N. H. Shah, E. Eryilmaz, D. Cowburn, T. W. Muir, Extein residues play an intimate role in the rate-limiting step of protein trans-splicing. *J. Am. Chem. Soc.* **135**, 5839–5847 (2013). doi:10.1021/ja401015p Medline

51. M. Tormen, E. Sovernigo, A. Pozzato, M. Pianigiani, M. Tormen, Sub-100 μs nanoimprint lithography at wafer scale. *Microelectron. Eng.* **141**, 21–26 (2015). doi:10.1016/j.mee.2015.01.002

52. T. Cordes, J. Vogelsang, P. Tinnefeld, On the mechanism of Trolox as antiblinking and antibleaching reagent. *J. Am. Chem. Soc.* **131**, 5018–5019 (2009). doi:10.1021/ja809117z Medline

53. A. D. Edelstein, M. A. Tsuchida, N. Amodaj, H. Pinkard, R. D. Vale, N. Stuurman, Advanced methods of microscope control using μManager software. *J. Biol. Methods* **1**, e10 (2014). doi:10.14440/jbm.2014.36 Medline

54. K. Li, "The image stabilizer plugin for ImageJ" (February 2008); http://www.cs.cmu.edu/~kangli/code/Image_Stabilizer.html.